Electro, Physical & Theoretical Chemistry

The Adsorption of Chlorofluoromethane on Pristine, Al-, Ga-, P-, and As-doped Boron Nitride Nanotubes: A PBC-DFT, NBO, and QTAIM Study

Mohsen Doust Mohammadi[a] and Hewa Y. Abdullah*[b]

The feasibility of detecting a Chlorofluoromethane (CFM) gas molecule on the outer surface of a pristine single-walled boron nitride nanotube as well as Al-, Ga-, P-, and As-doped structures. A periodic boundary condition (PBC), within a density functional theory (DFT) method, using the Perdew, Burke, and Ernzerhof exchange-correlation (PBE0) functional, together with a 6-311G(d) basis set was used. Subsequently, the B3LYP, CAM–B3LYP, ωB97XD, and M06-2X functionals were also employed to consider the single point energies. Natural bond orbital (NBO) and quantum theory of atoms in molecules (QTAIM) were implemented by using the PBE0/6-311G(d). To explore the nature of the intermolecular interactions, density of state (DOS), Wiberg bond index (WBI), natural charge, natural electron configuration, donor–acceptor natural bond orbital interactions, the second-order perturbation energies tests, and noncovalent interaction (NCI) analysis are performed. The sensitivity of the adsorption will be increased when the gas molecule interacts with decorated nanotubes; therefore, the change of electronic properties can be used to design suitable nanosensors.

1. Introduction

Nanotubes are structurally divided into carbon and non-carbon nanotubes. Carbon nanotubes (CNTs) were first discovered independently by Iijima and Ichihashi in 1991 in soot from carbon discharge in a neon-containing medium.[1] CNTs can pass through cell walls because of their needle shape.[2] Various studies have shown that single-walled nanotubes are potentially very good agents for the delivery of anticancer treatments.[3] However, the toxicity of CNTs to tissues is still being studied.[4] Since the discovery of CNTs, many efforts have been made to discover non-CNTs due to the dependence of the properties of CNTs on the nanotube diameter and chiral features. Boron nitride nanotubes (BNNTs) were first synthesized in 1995.[5] And similar to their carbon counterparts, have excellent mechanical properties due to the strong sp3 bonds in the nanotube walls.[6]

BNNTs are characterized by remarkable mechanical and electrical properties, such as a wide band gap (3.5–5.5 eV),[7] good piezoelectric properties, high thermal and chemical stability,[8] and high oxidation resistance.[9] Their unique mechanical properties and high thermal conductivity,[10] are invaluable for diagnostic and therapeutic approaches to diseases as well as sensor-based applications. BNNTs are hydrophobic, insoluble in water, and their resistance to oxidation makes them useful as drug carriers.[11] In addition, BNNTs are non-toxic to cells and do not damage the DNA.[12] Ciofani et al. tested the non-toxicity of BNNTs,[13] with results showing that the chemical neutrality and structural stability of these nanotubes is attributable to their biocompatibility.[14]

Following the discovery of BNNTs in 1994 by Rubio et al.[15] and their synthesis by Chopra et al. in 1995,[5,16] Deca et al. studied the interactions between the (10, 0) and (10, 5) nanotubes with the drug molecule isoniazid (INH).[17] They showed that the binding energy of INH to BNNT (5, 5) was slightly more significant than that of BNNT (10, 0). Mukhopadhyay et al. studied the adsorption of tryptophan (a non-polar amino acid), sparic acid, and arginine (a polar amino acid) on BNNTs, and reported a strong bonding energy for the adsorption of the polar amino acid on the BNNT surface.[18] Peyghan et al. investigated the absorption and electrical structure of the BNNT (6, 0) imidazole molecule in the gaseous and soluble phases. They found that imidazole adsorption had no significant effect on the electrical structure of the BNNT.[19] Yang et al. studied the interaction between BNNTs with biological molecules using density-functional theory (DFT) calculation.[20] Anota et al. investigated the interaction between BNNT and metformin using DFT.[21] Recently, the interaction between the uracil molecule and BNNT (n, 0) was investigated by Mirzai et al.[22] Given the widespread use of BNNTs, many theoretical investigations have been conducted on the adsorption of different molecules onto the surface of various nanostructures, such as aluminum nitride and silicon carbide.[23]

Chlorofluoromethane (CFM), (also is known as Freon 31 or HCFC 31 with chemical formula CH_2ClF), is classified as a category 2 carcinogen from the group of chlorofluorocarbons

[a] Dr. M. Doust Mohammadi
School of Chemistry, College of Science
University of Tehran
Tehran 14176, Iran
[b] Dr. H. Y. Abdullah
Physics Education Department, Faculty of Education
Tishk International University
Erbil 44001, Iraq
E-mail: hewayaseen@gmail.com

Supporting information for this article is available on the WWW under https://doi.org/10.1002/slct.202003367

or dihalomethanes. It is a colorless, odorless, flammable gas with a solid monoclinic crystal structure of space group P21.[24] Chlorofluoromethane was used as the refrigerant. It is listed in the Montreal Protocol as a substance that degrades the ozone layer.[25] A rotational study has been performed by Caminati et al.[26] to investigate the dimer interactions of CFM molecule and the results confirm that the interactions are non-covalent. According to the dissociation energy of dimer complex of CMF molecule reported in,[26] we considered it as an isolated single molecule in this work.

In the present study, the interaction of CFM with BNNT and BN nanotubes doped with Al, Ga, P and As elements was studied. The structure of BN was optimized using Gaussian software to study the chemical stability and conductivity, the elements doping process on this nanotube have been studied. Because of the high sensitivity of computation to precisely determine the energy of molecular orbitals to investigate the conductivity and probability of physical and chemical adsorption, different structures need to be optimized using appropriate computational methods. For this purpose, the Perdew, Burke, and Ernzerhof (PBE0) functional and 6–311G (d) basis set was used in this research for computation. The B3LYP, CAM–B3LYP, ωB97XD, and M06-2X functionals with 6–311G (d) basis set were also used to calculate the single point energies. Natural bond orbital (NBO) and quantum theory of atoms in molecules (QTAIM) were studied by using the PBE0/6-311G (d) method and the results were used to obtain various physical parameters.

2. Result and Discussion

2.1. The structural analysis

To optimize the structure of pristine armchair (5,5) single walled BNNTs using periodic boundary conditions, we first considered a base cell of B and N atoms ($B_{20}N_{20}$) whose length (and diameter) is 5.038 Å (and 6.87 Å). Unlike the nanosheet, the nanotube was expanded in one direction only. We optimized this cell using the 1D periodic boundary condition DFT method with the PBE0 functional together with the basis set 6–311G (d). A 5×1×1 k-point sampling in the Brillion zone was employed in such a way that, by increasing the number of unit cells, the gradient of the absolute value of the total dipole moment and the total energy became minimal. After optimization of the pristine unite cell we substituted Al and Ga with B atom and P and As with the N atom. The optimization process was then repeated for the doped nanotubes. The quantitative bond lengths are shown in Figure 1.

The next step involved the optimization of the CFM/nanotube complexes. In this step, the CFM molecule was placed on the outer surface of each above-mentioned unit cell with a vertical distance of approximately 2.1 Å. To find the optimum distances between the nanotube and the CFM molecule we used the rigid scan and estimated the most efficient distance for some cases. It should be noted that we used the PBE0/6-311G (d) level theory for both the optimization and the rigid scan. To better explain the details of the adsorption process, compare Figures 1 and 2.

The BNNT is composed of several symmetric hexagons with four different adsorption positions for the adsorption of any molecule onto the outer surface of the nanotube as shown in Figure 3: on the B atom (T_1); on the N atom (T_2); on the B–N bond (T_3); and at the hexagonal center (T_4). The logical approach is to place the CFM molecule in each of these positions and measure the amount of adsorption energy (E_{ads}). It is important to note that the CFM molecule has different heads (H,Cl, and F), and that each of these heads must be placed at the desired position on the nanotube to measure the amount of absorption energy. Our experience shows a negligible difference exists in the amount of adsorption energies when we place the gas molecule in different directions on the nanotube. As mentioned in literature,[27] when the differences in the adsorption energies are "below the range of chemical interest," placing the CFM molecule from different heads in the different positions on the nanotubes provides identical results. To confirm this, we placed the CFM molecule from the F-head in the desired positions on the BN nanotube. The results showed a negligible difference among the

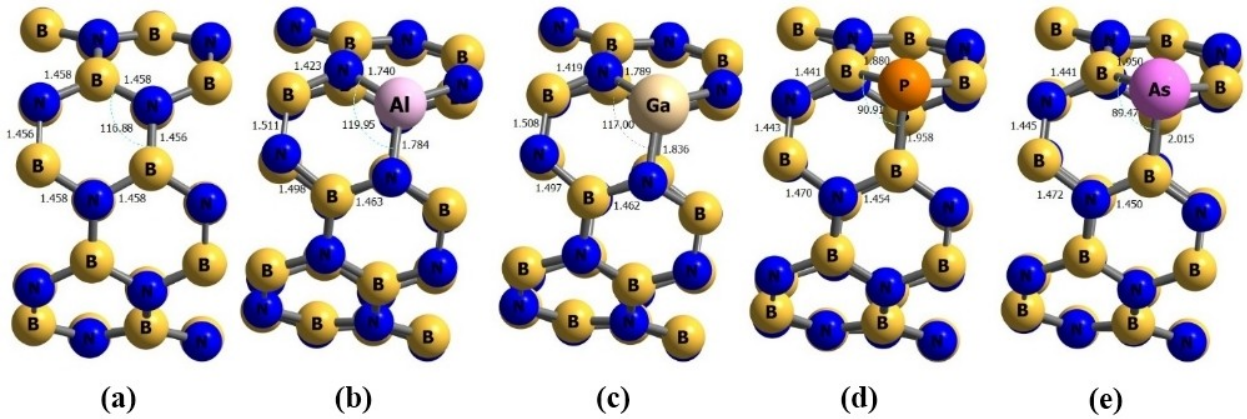

Figure 1. Unit cell structures of the (a) BNNT, (b) BNAlNT, (c) BNGaNT, (d) BNPNT, and (e) BNAsNT systems. The optimization process was performed using the PBE0/6-311G (d) level of theory. All quantitative values are in angstrom (Å).

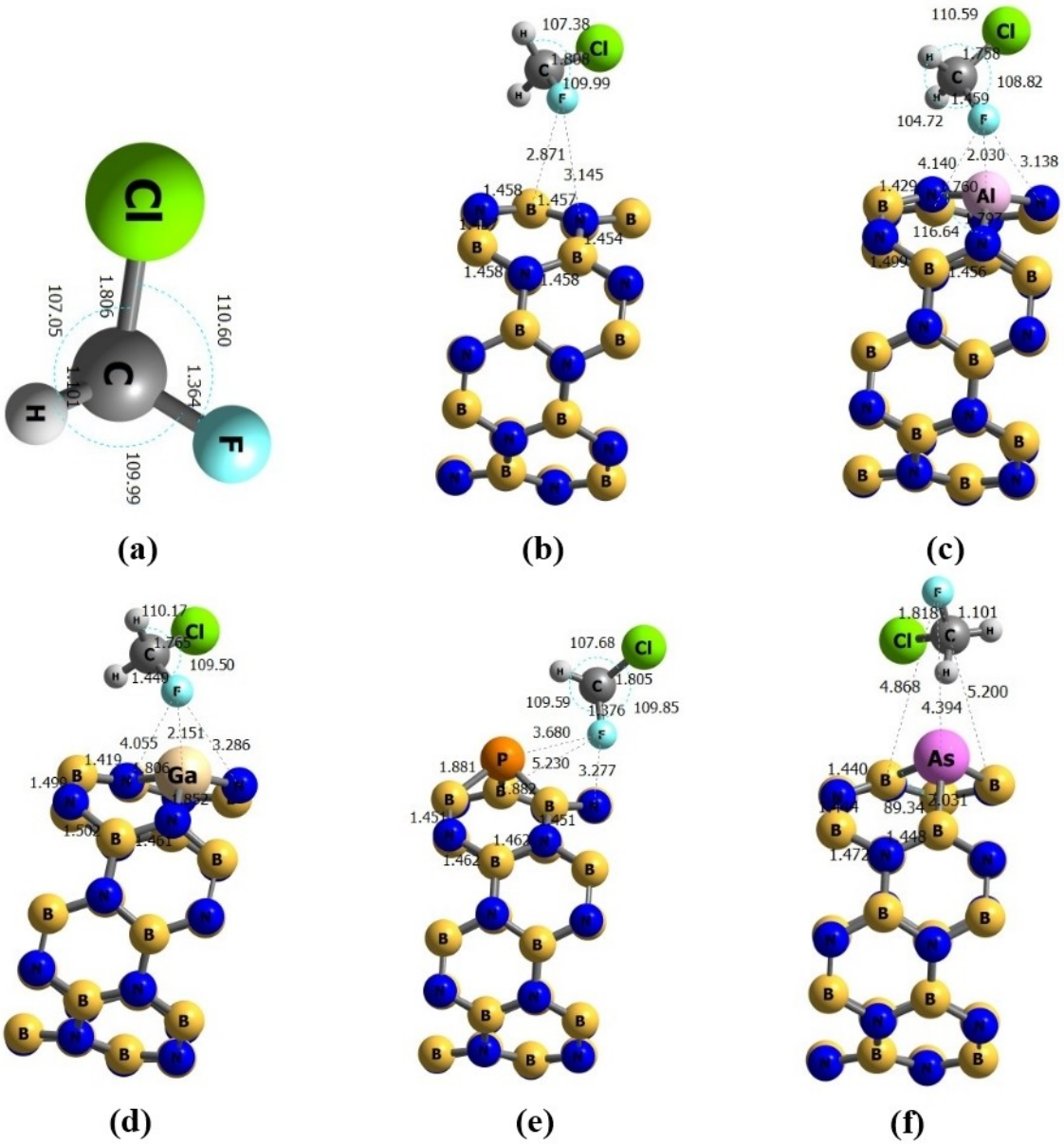

Figure 2. The most stable form of (a) isolated CFM and the adsorbed CFM molecule onto the outer surface of (b) BNNT, (c) BNAlNT, (d) BNGaNT, (e) BNPNT, and (f) BNAsNT. All clusters have been optimized using the PBE0 functional and 6–311G(d) basis set. All quantitative values are in angstrom (Å).

adsorption energies; therefore, the position of the B atom was chosen as the target position on the BN nanotube. Table S1 shows the energy difference (ΔE) between all possible adsorption sites (T_x) and the most stable configuration.

The optimization process on CFM/nanotube complexes in different orientations was performed to find the related local minima. Among this local minima, the most energetically stable complex was selected for NBO, QTAIM, analyses as well as single point energy calculations. To check the dispersion effect we only performed single point energy calculations. The results show our calculations are not method dependence and the same trend of adsorption energies repeats at any level of theory. Next, we extended the unit cell to five units and terminated them with hydrogen atoms (Figure 4) and the nanotube length for $B_{100}N_{100}H_{20}$ increased to 27.193Å. The single point energy calculations using different functionals B3LYP,[28] CAM–B3LYP,[29] ωB97XD,[30] and M06-2X,[31] and the 6–311G (d) basis set were performed. The calculated values indicated strong interactions between the nanotubes and the CFM molecule. Since the PBE0 functional does not account for the long-range scattering contribution, it is expected that in poor interactions, this functional will not provide a good estimate of the amount of energy. For this reason, methods have been developed to calculate these effects. In this work we used CAM–B3LYP and ωB97XD to consider long range and dispersion effects. The well-known B3LYP hybrid and M06-2X functionals were used to allow for good comparison. The results of the energy calculation of the systems studied using

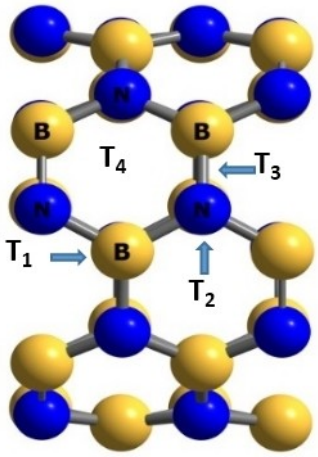

Figure 3. All possible target positions for the adsorption of any arbitrary molecules onto the surface of BNNT. Top of the B atom (T_1), top of the N atom (T_2), between the B and N atoms (T_3), and top of the hexagonal ring (T_4).

the above-mentioned levels of theory are reported in Table 1. In addition, the deformation energies are reported in Table S2.

The results show that the energies obtained from the PBE0-PBE0 and other functionals are consistent with the accuracy of the calculations. On the other hand, as expected, the ωB97XD method showed higher energy values due to the consideration of the contribution of dispersion. Moreover, doping the Al, Ga, P, and As elements on the BN nanotubes led to, significant changes in the results. Table 1 shows that doping using As and P, as well as Al and Ga, increased the absorption energy and enhanced the chemical absorption.

2.2. Energetics properties

The values of the HOMO and LUMO, and their differences (the HOMO–LUMO gap or HLG), chemical potential (μ), chemical hardness (η), and electrophilicity (ω) are reported in Table 2. It can be seen that adsorption of the CFM molecule onto the outer surface of the nanotubes reduced the distance between the HOMO and LUMO levels relative to the corresponding value for the pure nanotube. The greatest decrease was observed in the interaction of the Al-doped BNNT and CFM, which was caused by the molecular energy absorption matched from this position. Doping with Al, Ga, P, and As decreased HLG. The decrease in HLG increased the electrical conductivity, thereby

Table 1. The adsorption energies (E_{ads}) for the nanotube (NT) and CFM molecule. All values are in (eV).

Systems	PBE0	B3LYP	CAM–B3LYP	M06-2X	ωB97XD
CH_2ClF/BNNT	−1.040	−0.779	−1.105	−1.302	−1.727
CH_2ClF/BN(Al)NT	−4.157	−3.823	−4.477	−4.818	−4.936
CH_2ClF/BN(Ga)NT	−4.161	−3.754	−4.526	−5.506	−5.336
CH_2ClF/BN(P)NT	−1.244	−0.971	−1.338	−1.713	−1.914
CH_2ClF/BN(As)NT	−1.965	−1.671	−1.889	−2.249	−2.736

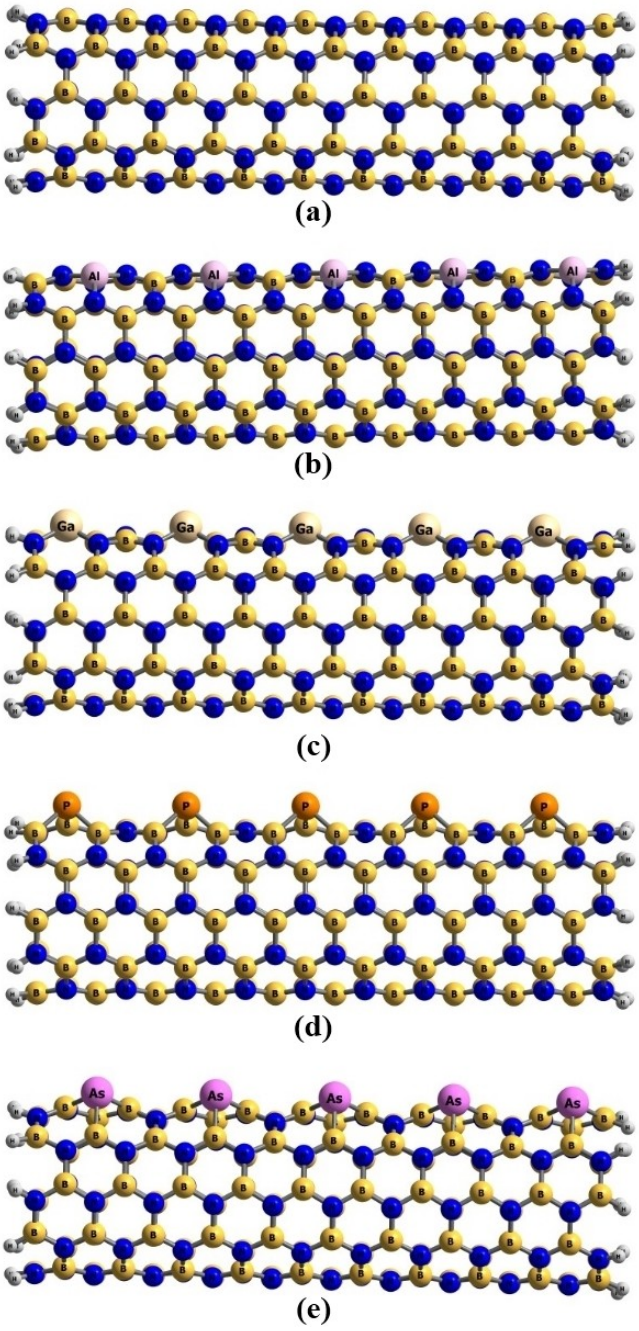

Figure 4. Expanded (a) BN, (b) Al-doped BN, (c) Ga-doped BN, (d) P-doped BN, and (e) As-doped BNNTs terminated with H atoms.

increasing the metal properties of all the nanotubes compared to the case of the pure BNNT. Moreover, note that the observed changes in HLG after doping with Al, Ga, P, and As were mainly due to the lower LUMO energy levels, and these changes were greater for metallic elements than the non-metallic ones. After the absorption of BCF, HLG of the nanotubes doped with Al and Ga increased, it decreased for the nanotubes doped with non-metallic elements (P and As). In order to study these changes in the electron structures more closely, the density of state (DOS) spectra were analyzed (Figure S1-S5).

Table 2. HOMO energy (ε_H), LUMO energy (ε_L), HOMO and LUMO energy gap (HLG), chemical potential (μ), chemical hardness (η), and electrophilicity (ω). All values are in (eV) and were obtained using the PBE0/6-311G (d) level of theory.

Systems	ε_H	ε_L	HLG	μ	η	ω
BNNT	−5.578	−1.086	4.492	−3.332	2.246	12.468
BN(Al)NT	−5.452	−2.327	3.125	−3.889	1.563	11.820
BN(Ga)NT	−6.208	−2.944	3.264	−4.576	1.632	17.087
BN(P)NT	−5.542	−2.070	3.472	−3.806	1.736	12.576
BN(As)NT	−5.364	−2.131	3.233	−3.747	1.616	11.349
CH_2ClF/BNNT	−5.476	−1.133	4.342	−3.305	2.171	11.855
CH_2ClF/BN(Al)NT	−4.966	−2.009	2.956	−3.488	1.478	8.990
CH_2ClF/BN(Ga)NT	−5.045	−1.970	3.075	−3.508	1.538	9.459
CH_2ClF/BN(P)NT	−5.504	−2.140	3.363	−3.822	1.682	12.283
CH_2ClF/BN(As)NT	−5.551	−2.348	3.203	−3.950	1.601	12.491

The DOS spectra for all the absorptions agree with the values of the energy parameters reported in Table 2. The lowest adsorption energy occurred for the pristine nanotube, and the highest, for the adsorption of CFMonto the Al-doped BN nanotube. The majority of the changes were also observed in the DOS spectrum relative to the Ga-doped nanotube. In other words, the changes in the electron structure showed a direct relationship with the absorption energies. Given the amount of absorption energy, high binding energy, and structures of the DOS spectra obtained in all the cases, it is logical to conclude that the adsorption of the CFM molecule onto the BN, BN(Al), BN(Ga), BN(P), and BN(As) nanotubes was chemical in nature.[32] In other words, the electronic transfers were significant.

2.3. NBO analysis

We used (NBO) analysis as well as the PBE0 functional together with 6–311 g (d) basis set to perform the NBO calculations. The main idea behind natural atomic orbital (NAO) and (NBO) was developed by Weinhold et al.[33] The concept of bonded orbitals can be used to understand the distribution of electrons in atomic and molecular orbitals. Atomic charges and molecular bonds can be used to obtain these orbitals. In this method, an electron density matrix is used to both define the shapes of the atomic orbitals in the molecular environment and to obtain molecular bonds (electron density between atoms). NBO is defined as the following equation for σ bonding between atoms A and B:

$$\sigma_{AB} = C_A h_A + C_B h_B \quad (1)$$

where h_A and h_B are natural hybrids on the A and B atoms. In the covalent limit $C_A = C_B$ and at the ionic limit $C_A \gg C_B$ (if the electronegativity of A is greater than B). Each bonding NBO must be paired with a corresponding anti bonding NBO:

$$\sigma^*_{AB} = C_A h_A - C_B h_B \quad (2)$$

Binding orbital analysis is used to evaluate the effects of non-stationary effects such as anomeric effect, rotation barrier, hydrogen bonding, and so on. In the NBO analysis, molecular energy is divided into two parts: total energy (for non-stationary enters) and Lewis molecule energy (where super-conjugation does not occur, and the electrons are strongly bound in single bonds and pairs). The occupied NBOs describe the covalent effects in the molecule, while non-occupied NBOs are used to describe non-covalent effects. The most important non-occupied NBOs are anti-bond orbitals.

NBO analysis was used to calculate the bond length using the Wiberg method for a more detailed examination of the type of interactions. The following section presents these results. After studying the adsorption energy of the complexes, we examine the bond length and bond order of the molecule and the nanotube before and after the adsorption as well as by doping with the various elements. The bond length and bond order for these clusters are reported in Table 3 and 4. According to these tables, the length of the B–N bond increased after the molecule adsorbed onto the nanotube, indicating that adsorption occurred between the molecule and the nanotube, while the bond order decreased.

After the elements were doped, the bond length between the doped element and the nanotube changed so that the system was in equilibrium. Table 3 shows the bond length of the nanotube doped with Al, Ga, P, and As after interaction with the CFM molecule. It is evident that the bond length increases by doping the elements. This causes the nanotube to stabilize, and for this reason, these structures appear to be more likely to interact with the molecule. The observed increase in bond length can be attributed to the increase in the atomic radius of the doping elements because the doped atoms are larger than the N and B atoms.

Table 3. Bond lengths and nearest intermolecular distances (re (Å)) between the CFM molecule and BNNT, BNAlNT, BNGaNT, BNPNT, and BNAsNT. All calculations were performed using the PBC-DFT PBE0/6-311G (d) level of theory.

r_e (Å)	F….(x)	F….B	F….N	C….(x)	Cl….(x)	F….(x)
CH_2ClF/BNNT	–	2.871	3.145	–	–	–
CH_2ClF/BN(Al)NT	2.030	4.140	3.138	3.017	4.128	2.831
CH_2ClF/BN(Ga)NT	2.151	4.055	3.286	3.102	3.871	3.033
CH_2ClF/BN(P)NT	3.680	5.230	3.277	3.802	5.601	3.522
CH_2ClF/BN(As)NT	4.394	5.200	4.868	3.822	4.79617	2.726

Table 4. WBI, obtained for atomic bonds and intermolecular interactions between the CFM molecule and BNNT, BNAlNT, BNGaNT, BNPNT, and BNAsNT. All calculations were performed using the PBE0/6-311G(d) level of theory.

WBI	F….(x)	F….B	F….N	C….(x)	Cl….(x)	H….(x)
CH_2ClF/BNNT	–	0.028	0.003	–	–	–
CH_2ClF/BN(Al)NT	0.214	0.001	0.009	0.007	0.011	0.002
CH_2ClF/BN(Ga)NT	0.200	0.002	0.012	0.008	0.019	0.006
CH_2ClF/BN(P)NT	0.003	0.023	0.004	0.003	0.001	0.001
CH_2ClF/BN(As)NT	0.001	0.001	0.001	0.005	0.001	0.011

The WBI relates to the bond order properties: the larger the WBI, the stronger the covalent character. As per the results in Table 4, the strongest bond occurs between the F atom from the CFM molecule and the Al and Ga atoms from the BNAlNT and BNGaNT. The obtained WBI values are more consistent with weak van der Waals interactions, and therefore, the adsorption of CFM onto these nanotubes is a physisorption process. All result agrees well with the previously presented results on absorption energy.

The results of the NBO calculations shed light on the natural electron configuration and partial natural charge which are useful in the study of the character of the bond between the nanotubes and the CFM molecule. The NBO approach was implemented for all atoms in the pristine and doped cluster systems to reveal the quantities listed in Table 5. For semiconducting inorganic nanotubes such as those selected in this study the negative charges located on the atom possess more electronegativity. The charge transfer quantity between the CFM molecule and the nanotubes can also be used as a criterion to study the interaction of nanotube and CFM, such that the stronger the interaction the more the charge transfer between CFM and the nanotube. Table 5 shows that significant charge transfer must have occurred between the two species during the adsorption process.

In addition, the type of interaction between the nanotubes and CFM molecule will be described by implementing the natural electron configuration. The results in Table 5 clearly indicate that the valance configuration of the isolated CFM molecule and nanotubes as well as the valence configurations of the nanotube/CFM clusters increased. Therefore, the interactions of CFM with all the nanotubes can be classified as strong chemisorption.

Donor-acceptor interactions due to the delocalization of electrons form a Lewis-type donor (σ) to a non-Lewis-type acceptor (σ) NBOs in a $\sigma \rightarrow \sigma$ donor-acceptor interaction can be estimated from the second order perturbative NBO methods. The results of electron donor-acceptor electron configuration of the pristine BNNT and doped BN(Al), BN(Ga), BN(P), and BN(As) nanotubes are reported in Table 6 according to the most values of E2 (i.e. the most important interactions in terms of the electron transfer stability energies are reported). The existence of such interactions with the remarkable stability energies in this table shows that in all cases the doped atom was incorporated into the nanotube structure by chemical interaction and a stable structure was created.

The data in Table 6 show the most important interaction for the pristine nanotube, namely the electron transfer from the BD (B–N) bond as the electron donor to the BD*(C–F) bond as the receptor. This finding agrees with the results of the absorption energy as well as the other results examined thus far. The study of the doped complexes reveals that in the Al-complex, the Al electron pair is the Al receptor (Lewis acid) and the N-bonded electron pair is the amino group of the electron donor molecule (Lewis base). The highest electron-acceptor stabilization energy in all cases is due to the same interaction, which indicates the strong adsorption of the molecule onto the BN (Al) nanotube compared to the other cases.

2.4. QTAIM analysis

QTAIM is a powerful tool for studying the type and structure of bonds and intermolecular interactions. According to this theory, the critical point of the electron density, which can be a minimum point, a maximum point, or a saddle point, can fall into one of the following four categories: (1) *Atomic critical point* (ACP), which denotes the geometrical position of an atom or nucleus (other than hydrogen), and geometrically represents a local maximum point of electron density in all three directions of space; (2) *bond critical point* (BCP), which indicates a critical point related to a bond or physical or chemical interaction (in reality, this point represents a saddle point with two directions of maximum electron density and one direction of minimum electron density); (3) *ring critical point* (RCP), which denotes a ring or set of atoms forming a ring (geometrically, it is a saddle point with the minimum electron density in one direction and in the other two directions); and (4) *cage critical point* (CCP), which is observed when multiple rings form a cage (geometrically, this point is a local minimum point in all three directions of space). For the QTAIM analysis, it is necessary to know the electron density $\rho(r)$ and Laplacian electron density $\nabla^2 \rho(r)$.

In QTAIM analysis, λ_1 and λ_2 are negative, and $|\lambda_1| < |\lambda_2|$ for the BCP. In the form where λ_1 and λ_2 are perpendicular to the bonding path, $\lambda 3$ is a positive value along the bonding path. In topology analysis ρ (r) and $\nabla^2 \rho$ (r) play an important role in the segmentation and identification of different types of chemical interactions. A BCP with negative values $\nabla^2 \rho$ (r) and large values of ρ (r) (of order $> 10^{-1}$ a.u.) is defined as a shared (covalent) intermolecular interaction. Also, when $\nabla^2 \rho$ (r) is positive the interaction can be classified as of the non-substrate close-shell type (which include ionic and van der Waals interactions).[34] The elliptical bond (ε),[35] and the virial theorem,[36] are two other important factors in the classification of bonds. An elliptical bond actually represents the electron density preferentially accumulated on a plate containing the bond and is defined as follows:

$$\varepsilon = \frac{\lambda_1}{\lambda_2} - 1 \tag{3}$$

Where

$$|\lambda_1| > |\lambda_2| \tag{4}$$

Large values of ε indicate an unstable structure, and vice versa. Also based on the virial theorem,[34,36] the following relationship exists between the electron kinetic energy density G (r), the electron potential energy density V (r) and the $\nabla^2 \rho$ (r):

$$\frac{1}{4}\nabla^2\rho(r) = 2G(r) + V(r) \tag{5}$$

The balance between $G(r)$ and $V(r)$ reflects the nature of the interaction, and therefore, the ratio of $G/|V|$ can be used as an

Table 5. Natural electron configurations and natural charges (au) for the isolated CFM, pristine and Al,Ga,P, and As doped nanotubes and their complex structures. All values were calculated using the PBE0/6-311G(d) level of theory.

Systems	Atom	Natural Charge	Natural Electron Configuration
BNNT	B	1.14	[core]2S(0.45)2p(1.40)3p(0.01) 3d(0.01)
	N	−1.14	[core]2S(1.35)2p(4.78)
BN(Al)NT	B	1.12	[core]2S(0.46)2p(1.41)3p(0.01) 3d(0.01)
	N	−1.14	[core]2S(1.41)2p(4.93)3p(0.01)
	Al	1.96	[core]3S(0.44)3p(0.57)3d(0.02) 4p(0.01)
BN(Ga)NT	B	1.14	[core]2S(0.46)2p(1.42)3p(0.01) 3d(0.01)
	N	−1.31	[core]2S(1.40)2p(4.88)3p(0.01)
	Ga	1.72	[core]4S(0.63)4p(0.67)4d(0.01) 5p(0.01)
BN(P)NT	B	1.12	[core]2S(0.46)2p(1.40)3p(0.01) 3d(0.01)
	N	−1.14	[core]2S(1.36)2p(4.77)
	P	0.18	[core]3S(1.42)3p(3.42)3d(0.02) 4p(0.01)
BN(As)NT	B	1.14	[core]2S(0.46)2p(1.40)3p(0.01) 3d(0.01)
	N	−1.13	[core]2S(1.36)2p(4.77)
	As	0.25	[core]4S(1.47)4p(3.31)4d(0.01) 5p(0.01)
CH_2ClF/BNNT	B	1.14	[core]2S(0.45)2p(1.40)3p(0.01) 3d(0.01)
	N	−1.14	[core]2S(1.35)2p(4.78)
	C	−0.04	[core]2S(1.13)2p(2.88)3p(0.01) 3d(0.01)
	H	0.23	1S(0.77)
	Cl	−0.09	[core]3S(1.88)3p(5.20)3d(0.01) 4p(0.01)
	F	−0.32	[core]2S(1.85)2p(5.46)
CH_2ClF/BN(Al) NT	B	1.14	[core]2S(0.45)2p(1.40)3p(0.01) 3d(0.01)
	N	−1.39	[core]2S(1.35)2p(4.78)
	Al	1.97	[core]3S(0.42)3p(0.59)3d(0.02) 4p(0.01)
	C	−0.09	[core]2S(1.17)2p(2.90)3p(0.01) 3d(0.01)
	H	0.26	1S(0.74)
	Cl	0.02	[core]3S(1.86)3p(5.11)3d(0.01) 4p(0.01)
	F	−0.34	[core]2S(1.84)2p(5.49)
CH_2ClF/BN(Ga) NT	B	1.14	[core]2S(0.44)2p(1.42)3p(0.01) 3d(0.01)
	N	−1.39	[core]2S(1.40)2p(4.93)3p(0.01)
	Ga	1.74	[core]2S(0.44)2p(1.42)3p(0.01) 3d(0.01)
	C	−0.08	[core]2S(1.16)2p(2.91)3p(0.01) 3d(0.01)
	H	0.25	1S(0.75)
	Cl	0.01	[core]3S(1.86)3p(5.11)3d(0.01) 4p(0.01)
	F	−0.32	[core]2S(1.84)2p(5.47)
CH_2ClF/BN(P) NT	B	1.13	[core]2S(0.45)2p(1.40)3p(0.01) 3d(0.01)
	N	−1.14	[core]2S(1.35)2p(4.78)
	P	0.14	[core]3S(1.40)3p(3.44)3d(0.01) 4p(0.01)
	C	−0.04	[core]2S(1.13)2p(2.88)3p(0.01) 3d(0.01)
	H	0.23	1S(0.76)
	Cl	−0.08	[core]3S(1.87)3p(5.19)3d(0.01) 4p(0.01)
	F	−0.32	[core]2S(1.85)2p(5.46)
CH_2ClF/BN(As) NT	B	1.14	[core]2S(0.45)2p(1.40)3p(0.01) 3d(0.01)
	N	−1.13	[core]2S(1.35)2p(4.78)
	As	0.23	[core]4S(1.45)4p(3.31)4d(0.01)
	C	−0.02	[core]2S(1.12)2p(2.87)3p(0.01) 3d(0.01)
	H	0.21	1S(0.78)
	Cl	−0.10	[core]3S(1.88)3p(5.21)3d(0.01) 4p(0.01)
	F	−0.32	[core]2S(1.84)2p(5.47)
CH_2ClF	C	−0.04	[core]2S(1.13)2p(2.89)3p(0.01) 3d(0.01)
	H	0.22	1S(0.77)
	Cl	−0.32	[core]3S(1.88)3p(5.19)3d(0.01) 4p(0.01)
	F	−0.08	[core]2S(1.84)2p(5.47)

Table 6. Donor-acceptor NBO interactions and second order perturbation energies (*E*2) for CFM clusters with BNNT, BNAlNT, BNGaNT, BNPNT, and BNAsNT. All values were obtained from the completed nanotubes using the PBE0/6-311G (d) level of theory.

Systems	Donor NBO (i)	Acceptor NBO (j)	E2(kcal/mol)
CH_2ClF/BNNT	BD (B–N)	BD*(C–H)	0.2
	BD (B–N)	BD*(C–F)	0.1
	BD (B–N)	RY*(H)	0.06
	BD (B–N)	RY*(F)	0.05
CH_2ClF/BN(Al)NT	BD (B–N)	LP*(Al)	21.9
	BD (B–N)	RY*(Al)	1.09
CH_2ClF/BN(Ga)NT	BD (B–Ga)	BD*(C–F)	0.52
	BD (B–Ga)	BD*(C–H)	0.28
	BD (B–Ga)	RY*(H)	0.06
	BD (B–N)	BD*(C–H)	0.06
	BD (B–N)	RY*(H)	0.11
CH_2ClF/BN(P)NT	BD (B–N)	BD*(C–F)	0.06
CH_2ClF/BN(As)NT	BD (B–N)	RY*(Cl)	0.06
	BD (B–As)	BD*(C–H)	0.44
	BD (B–N)	RY*(H)	0.44

appropriate index in link classification. If this ratio is less than 0.5, the nature of the interaction will be purely covalent, and if the ratio is greater than 1, the interaction may be considered as completely non-covalent. Note that for covalent bonds (i.e. $\nabla^2\rho(r) < 0$ and $G/|V| < 0.5$), the nature of the bond change

from van der Waals interactions to strong covalent interactions. The values of ε can also play a decisive role in controlling the amount of ionic interaction for closed-shell interactions (i.e. $\nabla^2\rho(r)>0$ and $G/|V|>1$), such that with decreasing ε value the interactions are moved from weak van der Waals to strong ionic (electrostatic) character. The information obtained after optimizing the initial and doped nanotubes and their complexes using QTAIM analysis is reported in Table 7.

Table 7 shows important results. All the adsorption sites had positive values for the Laplacian of electron energy density (i.e. the bonds are non-covalent). The study of the doped systems showed that the energy densities and the Laplacian of electron energy densities were high for all clusters, indicating that a strong bond exists between the nanotubes and the CFM molecule, and the elliptical bond is close to 0. Thus, the interaction is strong. As stated above, when G/|V| exceeds 1, the bond is non-covalent, and in the case of Ga-doped cluster, this amount is less than 1. In other words, the results of the QTAIM analysis also confirm the chemical adsorption of the CFM molecule on BN(Ga)NT (Figure 5).

Reduced density gradient (RDG) and $\mathrm{sign}\lambda_2(r)\rho(r)$ are a pair of functions used in Noncovalent interaction (NCI) [64] analysis which can be implemented to visualize the region and the type of weak interactions. RDG is defined as follows:[37]

$$RDGs = \frac{1}{2(3\pi^2)^{\frac{1}{3}}}\frac{|\overrightarrow{\Delta\rho}(r)|}{\overline{\rho(r)}^{\frac{4}{3}}} \quad (5)$$

The noncovalent interactions can be characterized in the region with low electron density and low RDG. The strength of the interaction has a positive correlation with electron density $\rho(r)$ and the sign of the second eigenvalue of the electron density Hessian matrix ($\mathrm{sign}\lambda_2$). Thus, the real space function sign of $\lambda_2(r)\rho(r)$ (the products of the signs of λ_2 and ρ) can be defined. The scatter graph of the sign of the $\lambda_2(r)\rho(r)$ function (*X*-axis) and RDG (*Y*-axis) reveals the noncovalent interaction type between CFM and nanotubes. The RDG values range from medium to very large around the nuclei and edges of the molecules, whereas weak interactions (zero to medium) are observed around the chemical bonds. Also, for each specific value of RDG (seen as a horizontal line on the graph), the regions of the graph can be classified into three types, namely, $\mathrm{Sign}\lambda_2(r)\rho(r)<0$ (strong attraction), $\mathrm{sign}\lambda_2(r)\rho(r)\approx 0$ (weak van der Waals interaction), and $\mathrm{sign}\lambda_2(r)\rho(r)>0$ (strong repulsion (steric effect in ring)).[37]

Using the isosurface RDG = 0.5 as a reference, it can be concluded that after adsorption of the CFM molecule onto the outer surfaces of the nanotubes, spots appeared around the region characterized by $\mathrm{sign}\lambda_2(r)\rho(r)\approx 0$. The interactions of CFM with the nanotubes were strong in nature. Significant changes in the overall features of the pristine nanotubes graph after the adsorption of CFM were observed in the region characterized as $\mathrm{sign}\lambda_2(r)\rho(r)<0$ (i.e. strong attraction), implying that the nanotube/CFM interactions were stronger compared with those of the isolated nanotubes (figs. S6-S10). Hence, this analysis also confirms the results of the single-point energy calculations, QTAIM analysis, and NBO analysis, namely that the interactions of CFM with the pristine and doped nanotubes were strong.

3. Conclusion

In this study, the interactions between Chlorofluoromethane molecules and pristine, Al,Ga,P, and As-doped boron nitride nanotubes as were investigated using density functional framework. The structures of the nanotubes and CFM molecule were optimized using the PBE0-PBE0/6-311G (d) level of theory. The B3LYP, CAM–B3LYP, M062X, and wB97XD functionals and the same basis set were also used to consider the contribution of long range interactions and the dispersion effect. QTAIM and NBO analyses were implemented to consider the characteristics of the intermolecular interactions. The results of all the analyses were in agreement, and showed the following: (1) Among the different positions studied for pristine BNNT, position T_1 had the highest absorption energy; (2) Al, Ga, P, and As can be substituted by BNNT atoms via chemical bonding and, as binding elements, they can cause dramatic changes in the chemical, electronic and mechanical structure of the BNNT nanotubes. By injecting impurities into the nanotube, the molecular symmetry is disturbed, and thus the polarity of the molecule increases, which causes stronger adsorption to occur. On the other hand, because Ga and Al produce positive ions, Fluorine interacts with them more strongly than P and As; (3) Among the doped nanotubes, Ga-doped BNNT showed a very high adsorption energy compared to those of BNNT doped with other elements. The chemical adsorption in this case makes this doped BNNT a suitable sensor option. The next category concerns Al, for which the adsorption energy is higher than the initial state but lower than that of Ga. Also, due to their strong absorption, the P and As-doped nanotubes, may

Table 7. The AIM topological parameters, electron density ($\rho(r)$), Laplacian of electron density ($\nabla^2\rho(r)$), kinetic electron density *G*(r), potential electron density *V*(r), eigenvalues of Hessian matrix (λ) and bond ellipticity index (ε) at the BCPs of the CFM clusters with BNNT, BNAlNT, BNGaNT, BNPNT, and BNAsNT. All values were calculated using the PBE0/6-311G(d) level of theory and NBO analysis.

Systems	Bond	ρ	$\nabla^2\rho$	$G(\rho)$	$V(\rho)$	$G(\rho)/V(\rho)$	λ_1	λ_2	λ_3	ε
CH_2ClF/BNNT	F….N	0.0086	0.0310	0.0069	−0.0060	1.1447	−0.0061	0.0405	−0.0034	0.8295
CH_2ClF/BN(Al)NT	F….Al	0.0363	0.2035	0.0504	−0.0499	1.0100	−0.0439	0.2924	−0.0450	0.0250
CH_2ClF/BN(Ga)NT	F….Ga	0.0471	0.1796	0.0540	−0.0632	0.8551	−0.0513	0.2842	−0.0533	0.0376
CH_2ClF/BN(P)NT	F….P	0.0036	0.0118	0.0022	−0.0014	1.5242	−0.0013	0.0136	−0.0006	0.2764
CH_2ClF/BN(As)NT	F…As	0.0108	0.0301	0.0064	−0.0053	1.2106	−0.0082	0.0469	−0.0086	0.0575

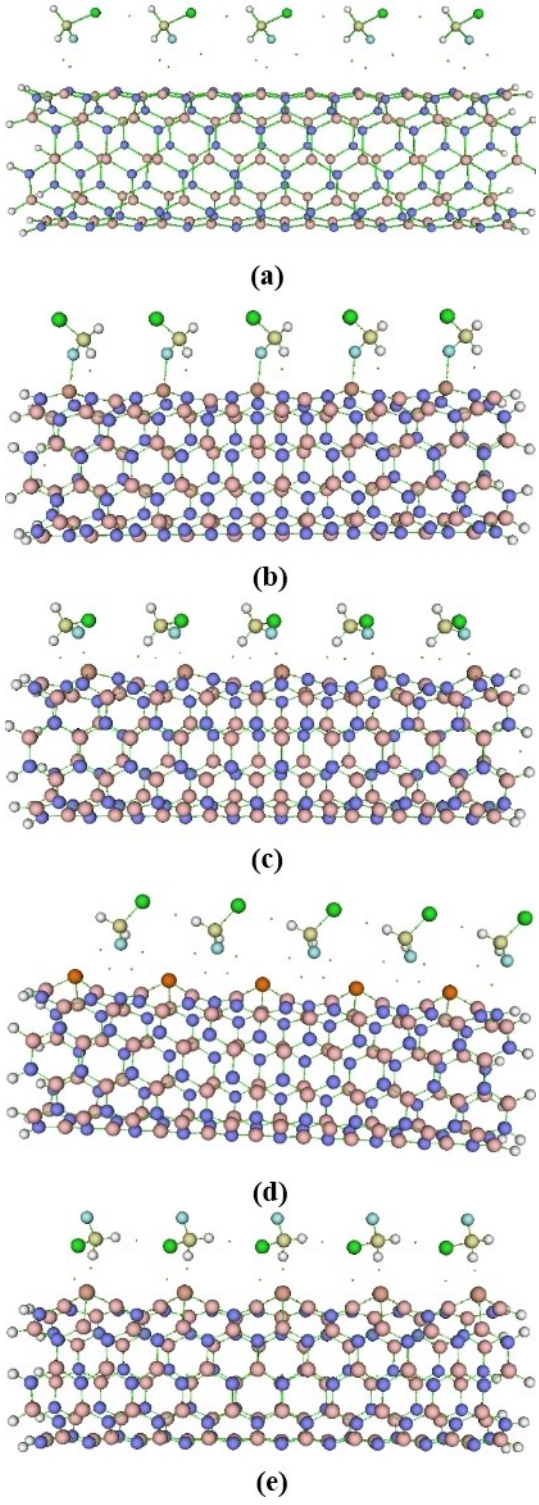

Figure 5. AIM molecular graphs for the (a) CFM/BNNT, (b) CFM/BNAlNT, (c) CFM/BNGaNT, (d) CFM/BNPNT, and (e) CFM/BNAsNT systems. The orange dots represent the (BCPs).

be better options than the pure BN nanotubes for designing suitable CFM nanosensors.

Supporting Information Summary

Computational details are available in SI.

Acknowledgements

I would like to thank the Solid-State Theory Group at the Physics Department at the Universita' degli Studi di Milano-Italy for providing computational facilities.

Conflict of Interest

The authors declare no conflict of interest.

Keywords: Boron Nitride · Chlorofluoromethane · Density Functional Theory · Freon 31 · Natural Bond Orbital

[1] M. Monthioux, V. L. Kuznetsov, *Carbon* **2006**, *44*, 1621–1623.
[2] M. Ghadamgahi, D. Ajloo, *J. Braz. Chem. Soc.* **2015**, *26*, 185–195.
[3] a) W. Wu, S. Wieckowski, G. Pastorin, M. Benincasa, C. Klumpp, J. P. Briand, R. Gennaro, M. Prato, A. Bianco, *Angew. Chem.* **2005**, *44*, 6358–6362; b) L. Wang, D. Zhu, L. Duan, W. Chen, *Carbon* **2010**, *48*, 3906–3915.
[4] V. Rastogi, P. Yadav, S. S. Bhattacharya, A. K. Mishra, N. Verma, A. Verma, J. K. Pandit, *J. Drug Delivery* **2014**, *2014*.
[5] N. G. Chopra, L. X. Benedict, V. H. Crespi, M. L. Cohen, S. G. Louie, A. Zettl, *Nature* **1995**, *377*, 135–138.
[6] a) W.-Q. Han, W. Mickelson, J. Cumings, A. Zettl, *Appl. Phys. Lett.* **2002**, *81*, 1110–1112; b) D. Golberg, Y. Bando, C. Tang, C. Zhi, *Adv. Mater.* **2007**, *19*, 2413–2432.
[7] X. Blase, A. Rubio, S. Louie, M. Cohen, *EPL* **1994**, *28*, 335.
[8] K. M. Liew, J. Yuan, *Nanotechnology* **2011**, *22*, 085701.
[9] a) D. Golberg, Y. Bando, K. Kurashima, T. Sato, *Scr. Mater.* **2001**, *44*, 1561–1565; b) S. M. Nakhmanson, A. Calzolari, V. Meunier, J. Bernholc, M. B. Nardelli, *Phys. Rev. B: Solid State* **2003**, *67*, 235406.
[10] C. Chang, A. Fennimore, A. Afanasiev, D. Okawa, T. Ikuno, H. Garcia, D. Li, A. Majumdar, A. Zettl, *Phys. Rev. Lett.* **2006**, *97*, 085901.
[11] Q. Weng, B. Wang, X. Wang, N. Hanagata, X. Li, D. Liu, X. Wang, X. Jiang, Y. Bando, D. Golberg, *ACS Nano* **2014**, *8*, 6123–6130.
[12] G. Ciofani, S. Danti, S. Nitti, B. Mazzolai, V. Mattoli, M. Giorgi, *Int. J. Pharm. (Amsterdam, Neth.)* **2013**, *444*, 85–88.
[13] a) G. Ciofani, V. Raffa, A. Menciassi, A. Cuschieri, *Biotechnol. Bioeng.* **2008**, *101*, 850–858; b) G. Ciofani, V. Raffa, A. Menciassi, A. Cuschieri, *Nanoscale Res. Lett.* **2009**, *4*, 113.
[14] C. Zhi, Y. Bando, C. Tang, D. Golberg, *Mater. Sci. Eng.* **2010**, *70*, 92–111.
[15] A. Rubio, J. L. Corkill, M. L. Cohen, *Phys. Rev. B: Solid State* **1994**, *49*, 5081.
[16] N. G. Chopra, R. Luyken, K. Cherrey, V. H. Crespi, M. L. Cohen, S. G. Louie, A. Zettl, *Science* **1995**, *269*, 966–967.
[17] N. Saikia, S. K. Pati, R. C. Deka, *Appl. Nanosci.* **2012**, *2*, 389–400.
[18] S. Mukhopadhyay, R. H. Scheicher, R. Pandey, S. P. Karna, *J. Phys. Chem. Lett.* **2011**, *2*, 2442–2447.
[19] A. A. Peyghan, M. T. Baei, M. Moghimi, S. Hashemian, *J. Cluster Sci.* **2013**, *24*, 31–47.
[20] C.-K. Yang, *Comput. Phys. Commun.* **2011**, *182*, 39–42.
[21] E. C. Anota, G. H. Cocoletzi, *Phys. E (Amsterdam, Neth.)* **2014**, *56*, 134–140.
[22] M. Mirzaei, *Superlattices Microstruct.* **2013**, *57*, 44–50.
[23] a) M. Abbasi, E. Nemati-Kande, M. D. Mohammadi, *Comput. Theor. Chem.* **2018**, *1132*, 1–11; b) M. D. Mohammadi, M. Hamzehloo, *Comput. Theor. Chem.* **2018**, *1144*, 26–37; c) E. Nemati-Kande, M. Abbasi, M. Doust Mohammadi, *ChemistrySelect* **2018**, *3*, 9833–9840; d) E. Nemati-Kande, M. Abbasi, M. D. Mohammadi, *ChemistrySelect* **2019**, *4*, 2453–2462; e) Z. Mahdavifar, Z. Nomresaz, E. Shakerzadeh, *Chem. Phys.* **2020**, *530*, 110606; f) N. Mohammadi-rad, M. D. Esrafili, J. J. Sardroodi, *J. Mol. Graphics Modell.* **2020**, 107537; g) E. Nemati-Kande, M. Abbasi, M. D.

Mohammadi, *J. Mol. Struct.* **2020**, *1199*, 126962; h) E. Nemati-Kande, R. Karimian, V. Goodarzi, E. Ghazizadeh, *Appl. Surf. Sci.* **2020**, *510*, 145490.
[24] O. S. Binbrek, B. H. Torrie, I. P. Swainson, *Acta Crystallogr. Sect. C* **2002**, *58*, o672-o674.
[25] U. N. E. P. O. Secretariat, *Handbook for the Montreal protocol on substances that deplete the ozone layer*, UNEP/Earthprint, **2006.**
[26] L. B. Favero, A. Maris, S. Melandri, P. Ottaviani, W. Caminati, *Phys. Chem. Chem. Phys.* **2019**, *21*, 3695–3700.
[27] J. Foresman, E. Frisch, *Gaussian Inc., Pittsburgh, Pennsylvania* **1996**.
[28] C. Lee, W. Yang, R. G. Parr, *Phys. Rev. B* **1988**, *37*, 785.
[29] a) T. Yanai, D. P. Tew, N. C. Handy, *Chem. Phys. Lett.* **2004**, *393*, 51–57; b) R. Kobayashi, R. D. Amos, *Chem. Phys. Lett.* **2006**, *420*, 106–109.
[30] J.-D. Chai, M. Head-Gordon, *Phys. Chem. Chem. Phys.* **2008**, *10*, 6615–6620.
[31] a) Y. Zhao, D. G. Truhlar, *J. Chem. Phys.* **2006**, *125*, 194101; b) R. L. Zhong, H. L. Xu, S. L. Sun, Y. Q. Qiu, Z. M. Su, *Chem. Eur. J.* **2012**, *18*, 11350–11355.
[32] J. J. Gilman, *Mater. Res. Innovations* **1997**, *1*, 71–76.
[33] J. Foster, F. Weinhold, *J. Am. Chem. Soc.* **1980**, *102*, 7211–7218.
[34] C. F. Matta, *Hydrogen Bonding-New Insights*, Springer, Berlin **2006**.
[35] H. J. Bohórquez, R. J. Boyd, C. F. Matta, *J. Phys. Chem. A* **2011**, *115*, 12991–12997.
[36] S. J. Grabowski, *J. Phys. Chem. A* **2012**, *116*, 1838–1845.
[37] a) E. R. Johnson, S. Keinan, P. Mori-Sánchez, J. Contreras-García, A. J. Cohen, W. Yang, *J. Am. Chem. Soc.* **2010**, *132*, 6498–6506; b) J. Contreras-García, E. R. Johnson, S. Keinan, R. Chaudret, J.-P. Piquemal, D. N. Beratan, W. Yang, *J. Chem. Theory Comput.* **2011**, *7*, 625–632.

Submitted: August 25, 2020
Accepted: October 7, 2020